Materials Science-Poland
Volume 42 Issue 3 · pp. 17–38 · DOI: 10.2478/msp-2024-0029

Materials Science-Poland

Compressive behavior of fiber-reinforced concrete strengthened with CFRP strips after exposure to temperature environments

Research Article

Aref A. Abadel*, Yousef R. Alharbi

Department of Civil Engineering, College of Engineering, King Saud University, Riyadh 11421, Saudi Arabia

Received 08 August 2024; Accepted 27 September 2024

Abstract: Reinforced concrete constructions are extremely vulnerable to fire damage over their lifespan. Despite its non-flammability, concrete is nonetheless affected by fire exposure, which impacts its stress–strain characteristics and durability. Therefore, developing strengthening methods is an economical option compared to the costs of demolishing and rebuilding constructions. This article aims to experimentally and numerically examine the strengthening of fiber-reinforced concrete cylinders by using carbon fiber-reinforced polymer (CFRP) strips after exposure to 600°C. Four different concrete mixtures have been investigated. A total of 48 cylinders were subjected to axial compression testing. The testing program primarily focused on three variables: (i) exposure temperature (600°C); (ii) the effect of using various types of fibers (steel fiber, polypropylene, and hybrid fibers); and (iii) CFRP strengthening. Finite element (FE) models were created using the ABAQUS program to conduct numerical analysis of concrete cylinders in exposure to heating scenarios and strengthen them with CFRP strips. The results show that when subjected to a temperature of 600°C, the compressive strength decreased significantly, ranging from 23.7 to 53.3%. The presence of fibers significantly impacted compressive strength, regardless of the fiber type, leading to an enhanced ratio of up to 34.7% in comparison to the control cylinders (i.e., unheated and unstrengthened cylinders). The suggested strengthening procedures using CFRP strips effectively repaired the heat-damaged cylinders, surpassing the initial compressive strength of unheated cylinders. The FE prediction shows satisfactory, consistent results in comparison to experimental data.

Keywords: *Concrete cylinder • CFRP • Compression strength • Elevated temperature • Finite element • Fiber-reinforced concrete • Strengthening*

1. Introduction

Concrete can be significantly affected by exposure to high temperatures, which can occur due to various environmental conditions such as fires. The extreme temperatures significantly contribute to structural degradation. Massive earthquakes have the potential to inflict significant damage upon reinforced concrete (RC) structures, resulting in inadequate lateral strength and a rapid decline in structural resilience. It is advisable to consider restoring and renovating the RC structural parts to limit potential damage in most circumstances. RC columns, which are the load-bearing components of all structures, are responsible for carrying both pure axial load and flexural bending moment, making them very crucial elements in buildings and bridges [1].

Concrete constructions can undergo significant deterioration when exposed to high temperatures. Many investigations were conducted to examine the effects of elevated temperatures on concrete members and methods to mitigate this degradation. Studies have investigated the residual compressive strength of cylinders after being subjected to fire at different temperatures [2]. A comprehensive examination of the effect of temperature on concrete strength reveals some noteworthy findings. The study carried out by Shaikh and Vimonsatit [3] demonstrated that compressive strength reduces when subjected to high temperatures, regardless of the cooling methods employed. In their study, Abadel et al. [4] investigated the effect of fiber-reinforced concrete (FRC) in various temperatures and

* *E-mail: aabadel@ksu.edu.sa*

cooling methods. The results indicate that FRC has superior residual strength compared with plain concrete. Li et al. [5] found that the compressive strength decreases considerably when subjected to temperatures between 400 and 600°C. Furthermore, studies have examined the static and dynamic mechanical characteristics of heat-damaged concrete cylinders, particularly for RC structures in nuclear reactors [6]. RC structures often have a comparatively high level of fire resistance, allowing them to withstand exposure to fire without suffering substantial damage. Studies indicate that conventional-strength concrete generally stays useful following fire accidents, although its durability may be reduced in a lifetime [7,8]. Hence, it is crucial to investigate techniques for repairing the affected areas or reinstating the structural integrity after a fire. Therefore, developing strengthening methods is an economical option compared to the costs of demolishing and rebuilding constructions.

Numerous studies have investigated the effects of elevated temperatures on the mechanical properties of FRC. For instance, Khaliq and Kodur [9] examined the thermal and mechanical properties of fiber-reinforced high-performance self-consolidating concrete at elevated temperatures. Their findings indicated that the addition of fibers significantly influenced the thermal behavior and mechanical performance, highlighting the potential of fiber reinforcement to mitigate strength loss at high temperatures. Novák and Kohoutková [10] examined the response of FRC to fire at high temperatures and found that the tensile and compressive strengths declined with increasing temperature. More precisely, researchers noted a decrease in compressive strength of 40% at 400°C and 65% at 600°C. They attributed this decline to higher levels of porosity and cracking that occur at elevated temperatures. A study conducted by Peng et al. [11] examined the impact of geometry and fiber type on fiber-reinforced high-strength concrete under high temperatures. Their findings demonstrated that organic fibers achieved a substantial reduction in pore pressure in concrete subjected to elevated temperatures. The fibers can be graded in terms of their effectiveness in reducing pore pressure as follows: polypropylene (PP), polyvinyl alcohol, and steel fibers (SFs).

The low tensile strength is considered the most significant drawback of conventional concrete. FRC, created by incorporating fibers into concrete, can address the drawback of conventional concrete [12,13]. FRC mixtures have superior mechanical characteristics compared to conventional concrete mixtures [14,15]. In the field of concrete engineering, a wide range of fiber types, such as steel, PP, and natural fibers, are commonly used. In addition to improving the tensile strength, the ductility, load-carrying capacity, flexural capacity, and flexural toughness of concrete were all significantly improved by the addition of fibers to the concrete mixture. Prior efforts have been made to utilize different types of fibers in cement-based composites to improve the ductility and toughness [16]. Most of the typical FRC products utilize a single type of fiber. The fracture bridging of the single fiber is restricted within a narrow range. Hence, a particular variety of fibers can potentially augment either the strength or ductility [17]. Therefore, it is necessary to combine fibers with different mechanical characteristics to create a cement-based composite that has improved strength and ductility. Hybrid FRC refers to cement-based composites that incorporate of two or more fiber types. The hybrid cement-based composite exhibits a synergistic response and derives advantages from all individual fiber properties [18]. Numerous investigations have shown that combining two or more types of fibers leads to increased ultimate strengths and strain-hardening behavior [19,20].

Column design should prioritize exhibiting ductile behavior. Fiber-reinforced polymer (FRP) composites are widely recognized by civil engineers as a highly effective technology for confining concrete. This strengthening technique enhances the concrete columns' ductility and load-bearing capability. Methods employed for enhancing and retrofitting structural integrity include the application of RC jackets, engineered cementitious composite, steel plates, aluminum strips, wire mesh integrated into mortar layers, and FRP in various configurations, including sheets, plates, or bars. In recent decades, there have been extensive investigations into various approaches and materials aimed at improving RC element production [21,22]. Ali Ahmed et al. [23] studied experimentally the performance and reliability of RC columns rehabilitated with FRP subjected to axial compression loading. The test results indicate that the strength for all repaired RC columns has been enhanced, regardless of the extent of initial damage. The increase in axial strength is inversely related to the extent of damage. Varma et al. [24] conducted an experimental and numerical study to examine the effects of compressive loads on concrete columns confined by natural FRP. Specifically, the strength and durability of concrete cylinders confined with epoxy composites made of basalt and jute fibers were assessed. Hybrid FRP wraps with jute and basalt fibers significantly improved load-bearing, energy absorption capacities, and confinement effectiveness compared to unconfined concrete columns in alkaline, acidic, potable water, and seawater environments. In recent years, advancements in science, particularly in civil engineering, have prompted researchers to exploit modern technologies, techniques, and artificial materials. Carbon fiber-reinforced polymer (CFRP) composites are

becoming increasingly popular among novel materials. CFRP composites exhibit advantageous characteristics in the automotive, aerospace, and construction sectors [25]. CFRP composites are developing greater importance because of their exceptional tensile strength, quick and effortless installation, resistance to corrosion, and impressive strength-to-weight ratio [26]. CFRP composites were initially employed in the mid-1980s to encase concrete columns to protect them from powerful earthquakes. Subsequently, CFRP composites were utilized to enhance the structural integrity of RC bridges in 1991. The occurrence of earthquakes in both Southern California and Kobe in 1990 and 1995, respectively, prompted additional research into the utilization of CFRP composites for RC structures in regions susceptible to earthquakes [1]. In recent decades, there have been many experimental experiments conducted on concrete specimens that were confined using different FRP composites [27,28]. These studies were intended to investigate the behavior of concrete specimens wrapped in different sizes of FRP under uniaxial compression. The experimental investigations were carried out to examine the effects of several characteristics, such as the strength of unconfined concrete, types, and layers of FRP composites. The test findings clearly showed that the use of FRP composites significantly enhanced the strength and ductility. Xiang et al. [29] investigated the effects of sulfate attack on square concrete columns strengthened with concrete canvas and CFRP sheets. The results indicated that using concrete canvas alleviated corner stresses, which led to improved CFRP utilization and averted localized failure.

According to the existing literature, there is a lack of knowledge regarding the compressive behavior of FRC that has been strengthened using CFRP strips after exposure to heating. This article aims to experimentally and numerically examine the efficiency of strengthening of FRC cylinders by using CFRP strips after exposure to 600°C. Four different concrete mixtures have been investigated. A total of 48 cylinders were subjected to axial compression testing. The testing program primarily focused on three variables: (i) exposure temperature (600°C); (ii) the effect of using various types of fiber (SF, PP, and hybrid fibers); and (iii) CFRP strengthening. In addition, finite element (FE) models were created using the FE program ABAQUS to conduct numerical analysis of concrete cylinders in exposure to heating scenarios and strengthen them with CFRP strips.

2. Experimental program

2.1 Material properties

This investigation utilized a normal-strength mixture containing coarse aggregates of 20 and 10 mm in size to achieve a compressive strength of cylinder specimens of 30 MPa within 28 days. The raw materials used to make each concrete mixture are as follows: (i) Type I ordinary Portland cement with a specific gravity of 3.15; (ii) crush sand with a specific gravity of 2.567%; (iii) silica sand with a fineness modulus and a specific gravity of 1.65 and 2.60, respectively; (iv) coarse aggregates with a specific gravity of 2.781%; and (v) a superplasticizer with a specific gravity of 1.21. All mixtures were combined with the superplasticizer to ensure consistent workability. The preparation of FRC involved the utilization of two types of fibers: (i) crimped polypropylene fibers (PPFs) and (ii) hooked-end SF, acquired from local suppliers. Figure 1 and Table 1

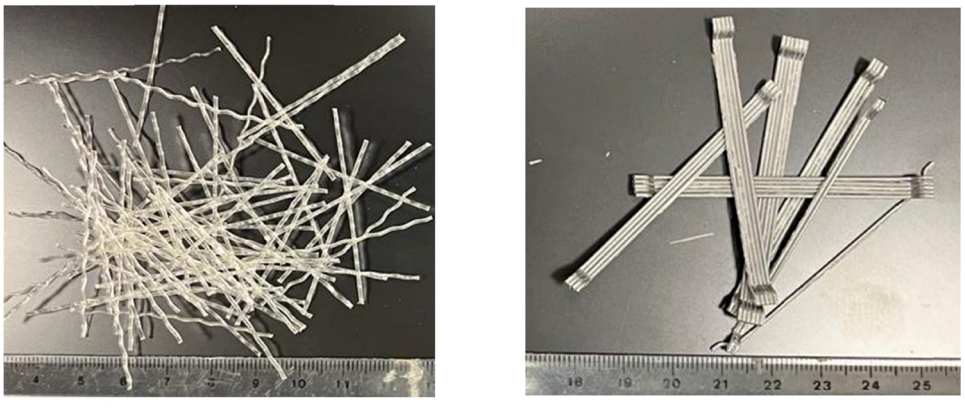

Figure 1. The fiber types: (a) PPF and (b) SF.

Properties	Fiber	
	PPF	SF
Shape	Crimped	Hooked ends
Section dimensions (mm)	1.0 × 0.6 (rectangular cross section)	0.75 (circular cross section)
Length (mm)	50	60
Tensile strength (MPa)	550	1225
Modulus of elasticity (Gpa)	4.0	200
Specific gravity	0.90	7.85

Table 1. Fiber characteristics.

illustrate the properties of the two types of fibers (i.e., SF and PPF) utilized in the study. The CFRP utilized in this investigation was a unidirectional carbon fiber fabric specifically designed for strengthening the structural elements. The HM-1803P epoxy adhesive resin was used, following the manufacturer's instructions. The HM-1803P is a two-part epoxy resin used for impregnation. Table 2 illustrates the characteristics of the epoxy adhesive and CFRP strip. The CFRP strip's tensile strength was assessed by performing tests on standard coupons following ASTM D3039 [30].

2.2 Mixture proportions

Table 3 displays the proportions of the components that are utilized in the preparation of mixtures. Table 4 displays the amounts of SF, PPF, or hybrid (i.e., SF + PPF) fibers in the concrete mixtures. This investigation involved the preparation of four mixtures of FRC. The control mixture (M-C0) was made without fibers, the second mixture (M-PPF) was made with SF fibers, the third mixture (M-SF) was made with PPF fibers, and the fourth mixture (M-SF + PPF) was made with both types of SF and PPF fibers. In addition, Table 4 displays the test matrix used in the experimental program of this investigation. Each test cylinder was replicated three times to assure data consistency and increase confidence in the study's conclusions. For this experiment, 48 cylinders (measuring 150 mm in diameter and 300 mm in height) were used. The testing program takes into account the following main variables: (i) the effectiveness of different types of fibers (SF, PPF, and hybrid fibers); (ii) heated damage (exposed to 26 and 600°C); and (iii) CFRP strip strengthening.

Material	Property	Value	Notes
CFRP strip	Tensile Young's modulus	68.9 GPa	Experimental values
	Thickness	1.0 mm	
	Tensile strength	1122 MPa	
	Tensile strain	1.7%	
Epoxy adhesive	Tensile strength	71.5 MPa	Given by the manufacturer
	Tensile Young's modulus	1.86 GPa	
	Tensile strain at break	%5.25	

Table 2. Epoxy adhesive and CFRP strip properties.

2.3 Specimen preparation

The concrete cylinders were cast using fabricated molds. To reduce the likelihood of segregation, the concrete paste was carefully and gradually (by three layers) cast into the fabricated molds. In addition, a vibrator was utilized to ensure the absence of any air voids. The concrete cylinders are positioned on the vibration table while being cast into the fabricated molds, as shown in Figure 2(a). The upper surface of the concrete cylinders was leveled, and a steel trowel was used to ensure a perfectly flat surface, thereby preventing the concentration of forces during the test. For 28 days, the cylinders were immersed in a water tank to undergo a curing procedure, as shown in Figure 2(b).

2.4 CFRP strengthening

Figure 3 shows the CFRP wrapping pattern applied in this study. The heat-damaged concrete cylinders were strengthened by applying CFRP strips, as shown in Figure 3. A single layer of CFRP strips was used, with a 75 mm overlap. Before installing the CFRP strip, the concrete cylinders were

Material		Weight
Ordinary Portland cement		378
Water		190.5
Silica sand		489
Crush sand		294
Coarse aggregate	$d_{agg.}$ = 20 mm	675
	$d_{agg.}$ = 10 mm	320
Super-plasticizer		1.0 L

Table 3. Concrete mixture proportions (in kg/m^3).

Mixture ID	Specimen ID	Temperature (°C)	Fiber volume			Strengthening	No. of specimens
			SF (%)	PPF (%)	Total (%)		
M-C0	C0-A	26	—	—	—	—	3
	C0-T	600					3
	C0-A-S	26				CFRP	3
	C0-T-S	600					3
M-PPF	PPF-A	26	—	0.2	0.2	—	3
	PPF-T	600					3
	PPF-A-S	26				CFRP	3
	PPF-T-S	600					3
M-SF	SF-A	26	0.6	—	0.6	—	3
	SF-T	600					3
	SF-A-S	26				CFRP	3
	SF-T-S	600					3
M-SF + PPF	SF + PPF-A	26	0.6	0.2	0.8	—	3
	SF + PPF-T	600					3
	SF + PPF-A-S	26				CFRP	3
	SF + PPF-T-S	600					3
			Total no. of specimens				48

Table 4. Test matrix used in the experimental program of this investigation.

subjected to surface roughening through the process of sandblasting. The goal was to ensure that the concrete cylinder surface and CFRP layer were fully bonded, as shown in Figure 2. The first step was a thorough cleaning of the concrete cylinder surface to remove any surface impurities, such as dust. Subsequently, an epoxy primer layer was

Figure 2. Methodology of experiments: casting, curing, heating, sandblasting, strengthening, and testing.

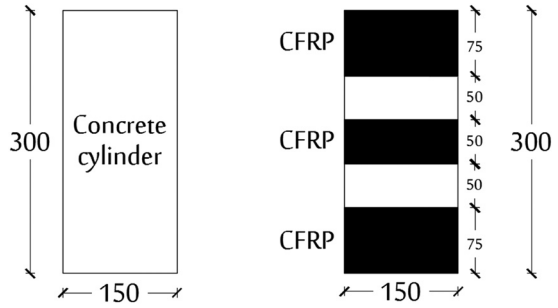

Figure 3. CFRP wrapping pattern.

applied to the surface of the cylinder. This was performed to eliminate any air voids on the surface of the cylinder and provide a fully bonded. Afterward, a thin coating of epoxy was applied. Subsequently, the CFRP laminates were precisely divided into strips of specified widths and lengths. The concrete cylinders were then carefully covered with the CFRP strip. The air trapped between the surfaces of the cylinder and CFRP strip was removed using a roller, allowing for more impregnation saturation. The concrete cylinders, after being strengthened with CFRP strips, are shown in Figure 2.

2.5 Heating of concrete cylinders

The concrete cylinders were exposed to heating in an electric oven (Figure 2) until they reached the target temperature of 600°C. As shown in Figure 2, some specimens were transferred from the lab to the oven the day before specimen testing was conducted. The specimens in the oven were subjected to a higher average heating rate of 8°C/min until reaching the temperature of 600°C. The specimens were placed in the oven and allowed to reach 600°C for 3 h before the oven was turned off. Afterward, the specimens were permitted to cool to the ambient temperature. Figure 4 shows the time–temperature curve utilized for a temperature exposure of 600°C, compared to the standard curve of ISO 834 [31]. Figure 4 also shows the cooling curve of specimens inside the oven. Then, the specimens were cooled by being left at room temperature for 24 h prior to testing.

2.6 Testing procedure

In this study, uniaxial compressive pressure was applied to the cylinders. Sulfur was applied to the specimen's upper surface to completely level it out during compression testing. Each concrete cylinder was attached to a compressometer to obtain the axial strain during the experimental test, as shown in Figure 2. Two linear variable differential transformers (LVDTs) were installed on two circular sleeves that encircled the concrete cylinder in the compressometer. To prevent the sleeves from influencing the dilatation of the concrete cylinder, they were securely attached to the cylinder using pin-type support. The wires of the LVDTs were linked to a data acquisition system, which was used to record the readings obtained throughout the experiment. Uniaxial compression was applied to each concrete cylinder until it failed. The compressive strength of the concrete cylinders was assessed using the approach specified in ASTM C39 [32].

3. Results and discussion

3.1 Failure modes

Figure 5 displays common failure patterns seen in strengthened and unstrengthened concrete cylinders after

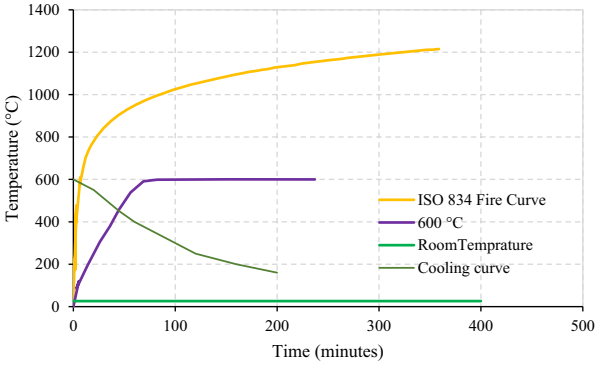

Figure 4. The heating and cooling curves used in this study.

undergoing compression testing and being subjected to heat at 600°C. The control specimens, which did not contain any fibers, experienced brittle failure as a result of concrete crushing, as illustrated in Figure 5. When exposed to high temperatures, the heat-damaged control specimens showed a decreased tendency toward brittle failure. Initially, the concrete cover displayed early signs of spalling. Consequently, a failure occurred when the axial load began to decrease, in contrast to specimens of the same type exposed to an ambient temperature (26°C). The concrete cylinders displayed a slight, visible change in color when subjected to a high temperature (600°C). Surface thermal cracking was seen on the concrete cylinders without fibers when subjected to a temperature of 600°C. Nevertheless, the pattern in which the heat-damaged cylinders failed was nearly identical to that of the unheated cylinders. The heat-damaged cylinders had a higher incidence of failures than the unheated cylinders. The C0-A cylinders display notable cracks and crushing, initially occurring at the top portion (i.e., the place of application of load) and subsequently at the midpoint of the cylinder. In the PPF-A cylinders, a similar pattern was noticed, with cracks originating from the loading point and extending toward the middle of the cylinder. This pattern differed from that observed in the SF-A and SF + PPF-A cylinders. However, the presence of fibers in the mixtures effectively reduced the occurrence of surface thermal cracks. The cylinders containing SF fibers (SF-A and SF + PPF-A) exhibited narrower crack widths compared to the cylinders without SF fibers (C0-A and PPF-A), as illustrated in Figure 5. The observed result can be related to the inclusion of SF, PPF, and hybrid fibers (SF + PPF) in the concrete cylinders, which provided a bridging effect across cracks, as reported in other studies (e.g., previous studies [33,34]). The fiber's presence can alter the failure pattern of concrete cylinders from brittle to ductile by improving their toughness, which is consistent with the findings of previous studies [35,36]. Typically, the cylinders without fibers experienced failure in an explosive or brittle manner. However, as a result of the random arrangement of fibers within the concrete matrix, the concrete cylinders containing fibers did not experience this phenomenon, resulting in reduced explosiveness or brittleness. The failure of heat-damaged cylinders with PPF fibers became more ductile. This phenomenon can be attributed to the PPF fibers' melting, which subsequently results in the formation of pores within the concrete core. Furthermore, in the heat-damaged concrete cylinders with SF fibers, the failure displayed enhanced ductility in comparison to cylinders without fibers. In addition, it exhibited a higher level of brittleness compared to those that had PPF fibers. The failure mechanism of heat-damaged concrete cylinders comprising hybrid fibers displayed intermediate characteristics between cylinders containing solely SF or PPF fibers. The failure pattern of the strengthened cylinders involved the rupture of the CFRP strips and the crushing of concrete. The cutout of the CFRP strips is linked to the ring-shaped rupture of the CFRP strip, as depicted in Figure 5. The CFRP strip in the middle portion ruptures in all the strengthened cylinders, as shown in Figure 5. Following the rupture of the CFRP, the adhesive strength was inadequate to withstand the tensile stress exerted by the radial expansion, followed by concrete crushing in the middle of the cylinder. Consequently, the debonding failure coincided with the CFRP rupture. Moreover, when exposed to similar temperatures, the strengthened cylinders exhibited improved ductility compared to the unstrengthened cylinders. Generally, the final failure mechanism of the concrete cylinders was significantly influenced by the strengthening of heat-damaged cylinders. Both strengthened cylinders (heated and unheated) had concrete crushing and CFRP rupture at the cylinder middle, as illustrated in Figure 5.

3.2 Effectiveness of using CFRP strips

Figure 6 displays the concrete compressive strength of all the cylinders. The results clearly indicate that the strengthening of concrete cylinders demonstrated higher compressive strength compared to the unstrengthened cylinders. This can be explained by increased confinement resulting from the existence of CFRP jackets. The unheated strengthened cylinders exhibited a significant improvement in compressive strength with increases of 59.1, 39.3, 54.1, and 32.1% for the C0-A-S, SF-A-S, PPF-A-S, and SF + PPF-A-S, respectively, in comparison with the control cylinders (i.e., unheated and unstrengthened cylinders) that were exposed to the same temperature: C0-A, SF-A, PPF-A, and SF + PPF-A, respectively. Regarding the strengthening of heat-damaged cylinders, the compressive strength increased by 114.2, 53.0, 96.1, and 29.8% for the C0-T-S, SF-T-S, PPF-T-S, and SF + PPF-T-S cylinders, respectively, compared to the heat-damaged control cylinders (i.e., heated and unstrengthened cylinders) C0-T, SF-T, PPF-T, and SF + PPF-T. Applying CFRP jackets to strengthen the heat-damaged cylinders led to a 0.1, 7.2, and 7.2% enhancement in compressive strength for C0-T-S, SF-T-S, and PPF-T-S cylinders, respectively, compared to the unheated cylinders C0-A, SF-A, and PPF-A. Nevertheless, the SF + PPF-T-S cylinders exhibited a marginal decline of 1.1% in comparison to SF + PPF-A, as depicted in Figure 6.

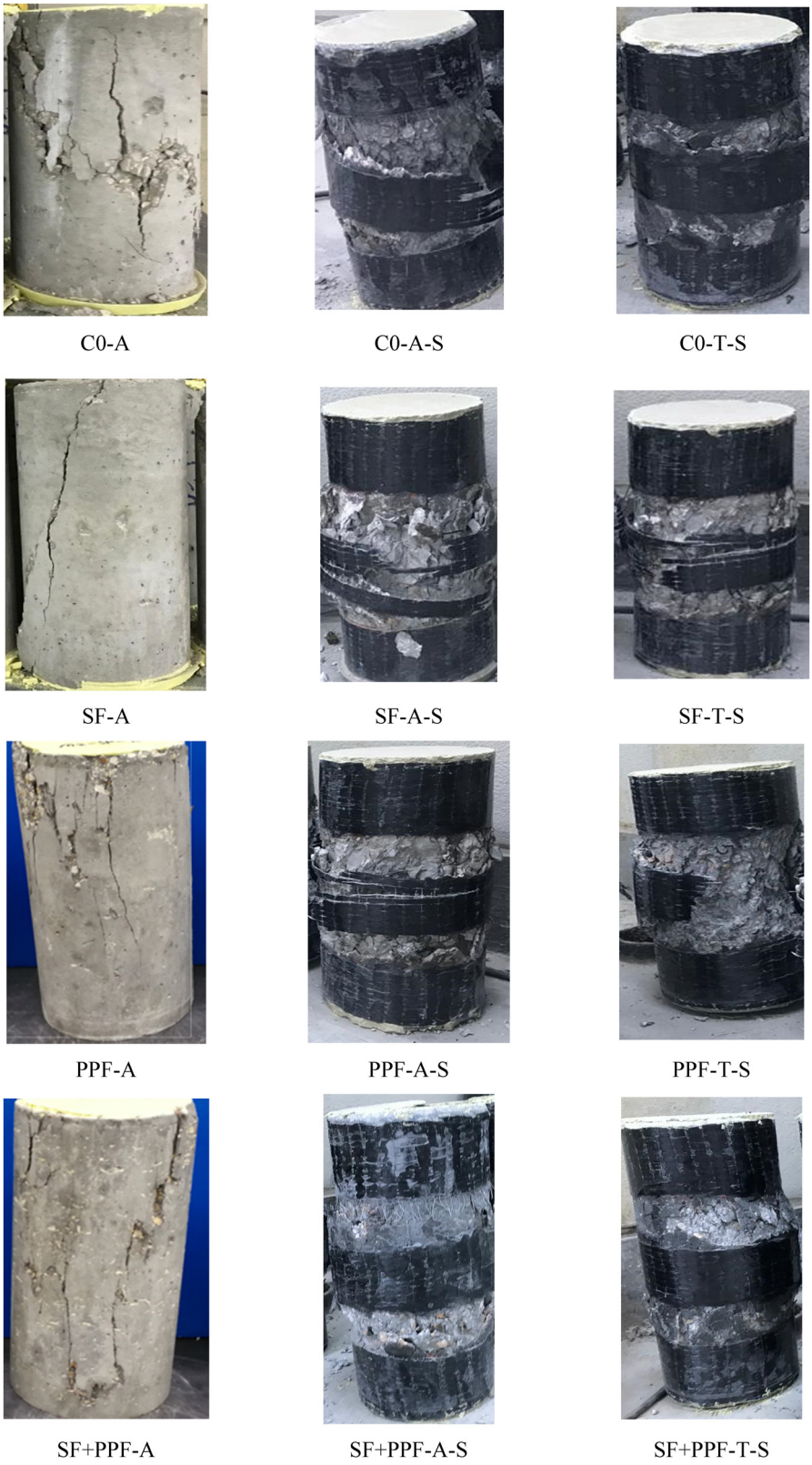

Figure 5. The failure patterns for strengthened and unstrengthened specimens.

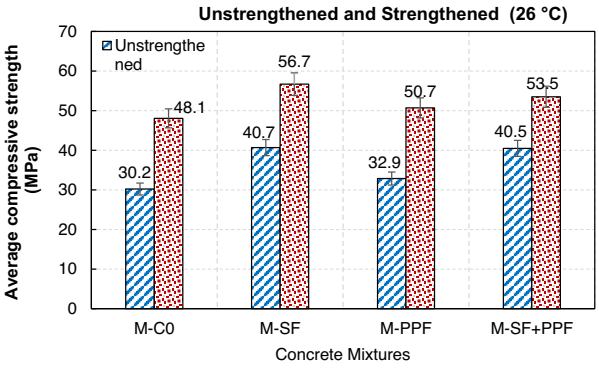

(a)

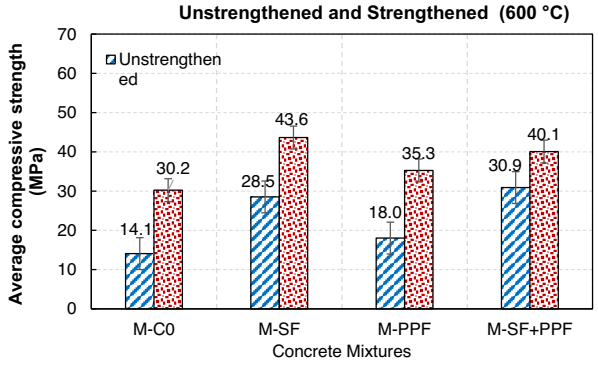

(b)

Figure 6. Effectiveness of CFRP jackets for all specimens at (a) 26°C and (b) 600°C.

3.3 Stress–strain curves

Figures 7(a) and 9(b) depict the stress–axial strain curves for heated (600°C) and unheated (26°C) concrete cylinders, respectively. The elastic modulus is reduced as the temperature increases from 26 to 600°C, as evidenced by the stress–axial strain curves. Figure 7(a) illustrates that the stress–axial strain curves of the unheated concrete cylinders have a predominantly linear pattern until they reach their peak stresses. The curves exhibited a decrease in incline, resulting in a non-linear response. Once the concrete cylinders reached their peak stresses, they began to develop cracks that gradually expanded, ultimately resulting in complete failure. A similar pattern was observed in the heated concrete cylinders. The curves for the unheated concrete cylinders exhibit a predominantly linear pattern until the maximum stresses, as depicted in Figure 7(b). The concrete cylinders containing SF or hybrid fibers exhibited a gradual decrease in the stress–axial strain curve. The capacity of the fibers to bridge the cracks led to improved ductility beyond the peak point, as illustrated in Figure 7. While the heated cylinders had a reduction in peak stress, the curves did not indicate an abrupt decline. Instead, they displayed virtually flat stress–axial strain curves (Figure 7(b)). The analysis of stress–axial strain curves reveals that the concrete cylinders, both with and without fiber, undergo a more significant decrease in initial stiffness than in compressive strength when subjected to a temperature of 600°C. The disintegration of the hydrated cement paste and the reduced moisture content are two factors that can explain the compressive strength reduction brought about by an increase in temperature. Additional researchers [4] have likewise established comparable results, demonstrating that the FRC mixture's strength experiences a notable decline when exposed to temperatures exceeding 600°C. Moreover, it is evident that the specimens containing SF fiber had a higher ability to absorb energy (as indicated by the area under curve) and a greater elastic modulus after being exposed to 600°C, when compared to the concrete cylinders without fibers, with PPF fibers, and those with hybrid fibers. The superiority of SF fibers over PPF fibers lies in their exceptional mechanical properties, such as elastic modulus and tension strength. Additionally, SF fibers have remarkable heat resistance, enabling them to sustain higher temperatures. PPF fibers, on the other hand, have the potential to melt when subjected to high temperatures. In addition, the reduction in the modulus of elasticity and ability to absorb energy due to heating was less in

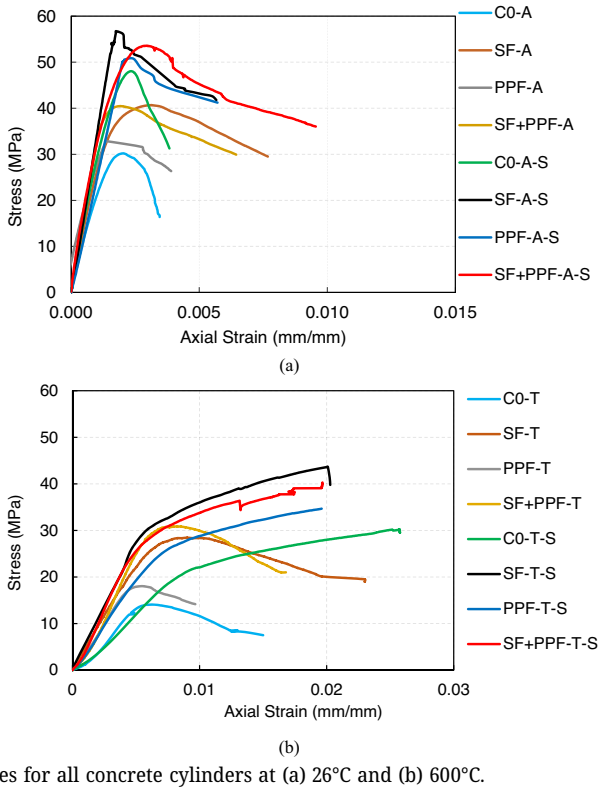

Figure 7. Stress–axial strain curves for all concrete cylinders at (a) 26°C and (b) 600°C.

concrete cylinders with hybrid fibers, as opposed to concrete cylinders solely with PPF fibers. The presence of SF fibers in the hybrid mixture improved the PPF fibers' weak points. Conversely, the inclusion of PPF fibers in the mixture resulted in a decrease in porosity [36]. The utilization of CFRP jackets significantly improved the peak strength, strain at peak stress, and post-peak behavior of all mixtures, irrespective of whether the cylinders were heated or unheated, as shown in Figure 7. Both SF and hybrid fiber concrete cylinders have demonstrated exceptional performance in comparison to other types of mixtures (i.e., C0 and PPF mixtures) under both strengthened and unstrengthened conditions. The influence of CFRP jackets was most evident when assessing the increase in maximum axial strains. The axial strains exhibited a substantial increase, with an average above 200%, in comparison to the strains of the unstrengthened concrete cylinders. The strengthened cylinders exhibited markedly higher performance in terms of enhancing maximum strain than the unstrengthened cylinders. After being subjected to high temperatures (600°C), the strengthened cylinders exhibited linear behavior in their stress–axial strain curves until reaching the peak stress, at which point there was a decrease in stress. Furthermore, it has been observed that the strengthened cylinders exhibited a greater capacity to absorb energy and displayed a more post-peak behavior following exposure to 600°C, in contrast to the cylinders that were not strengthened.

3.4 Effect of fiber types

Figure 8 displays the compressive strength of cylinders that were heated and unheated. The effect of fiber type on strength was previously reported in the author's earlier study [22]. It is included here for the sake of completeness and to provide additional information. The purpose is to assess the influence of different fiber types on the compressive strength after being exposed to 600°C. This relates to the concrete's residual strength following exposure to 600°C in comparison to its strength at 26°C (i.e., ambient temperature). The results indicate that the inclusion of fibers significantly influences the compressive strength, regardless of the type of fiber used. The inclusion of fibers effectively reduced the decrease in compressive strength resulting from exposure to 600°C in comparison to concrete mixtures without fibers. Therefore, this reduction in

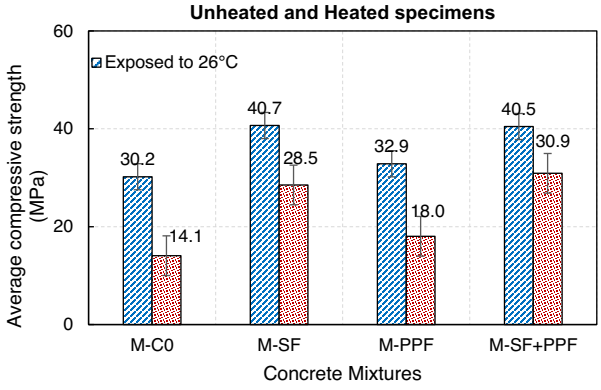

Figure 8. Effect of fiber types on compressive strength of concrete mixtures.

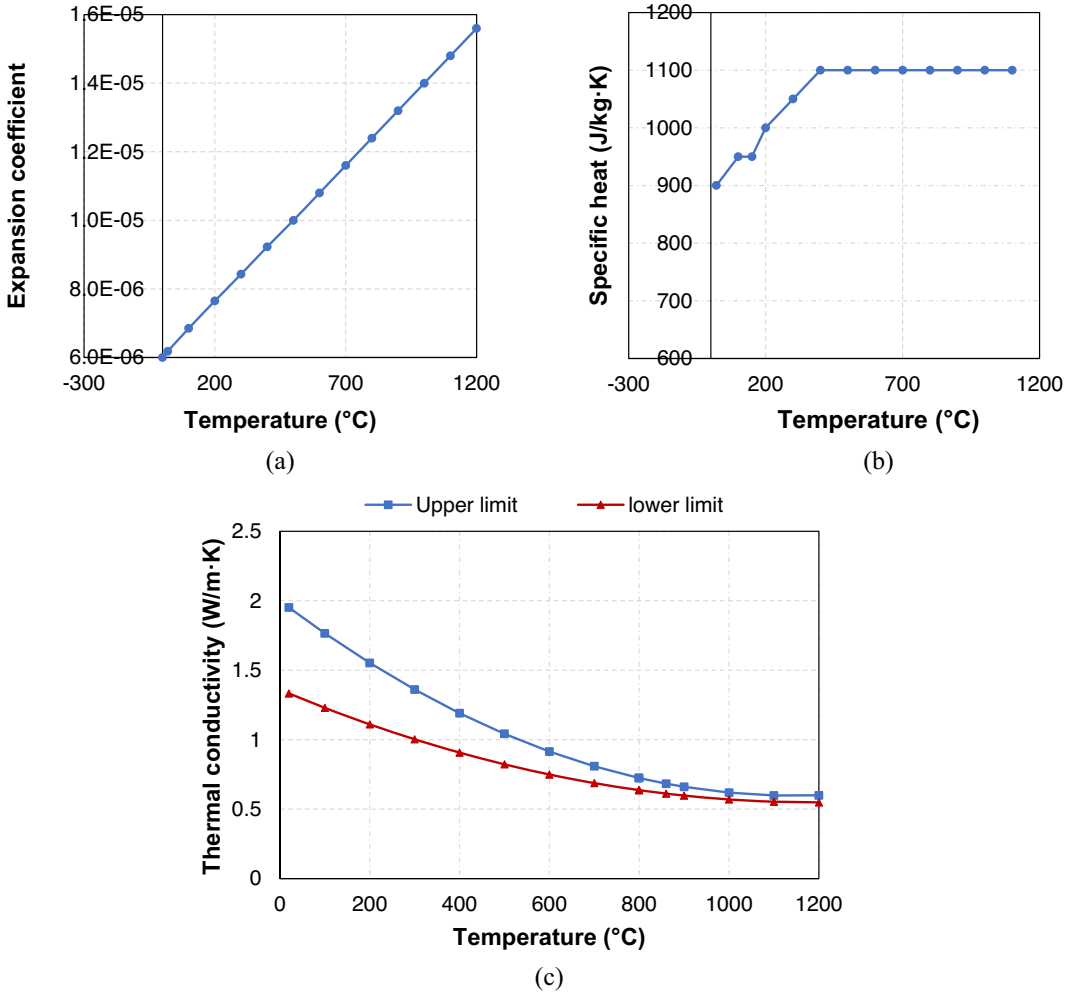

Figure 9. The concrete's thermal properties at various temperatures: (a) expansion coefficient, (b) specific heat, and (c) thermal conductivity.

the heat-damaged cylinders with fibers is less influential than the control concrete cylinders. The SF-A, PPF-A, and SF + PPF-A exhibited a higher ratio of 34.7, 8.9, and 34.1%, respectively, in comparison to the C0-A cylinders (i.e., control cylinders). The compressive strength of heat-damaged cylinders of C0-T, SF-T, PPF-T, and SF + PPF-T decreased by 53.3, 30.0, 45.3, and 23.7%, respectively, in comparison to unheated concrete cylinders of C0-A, SF-A, PPF-A, and SF + PPF-A. The main finding drawn from Figure 8 is that the fibers can be arranged according to their efficiency-enhancing potential: (i) inclusion of SF alone, (ii) inclusion of hybrid fibers, and (iii) inclusion of PPF alone. The SF fibers exhibit superiority due to their ability to create a bridging effect. The rationale behind this is that SF fibers exhibit exceptional mechanical characteristics, including a higher elastic modulus and tension strength, in comparison to PPF fibers. Moreover, SF fibers can endure elevated temperatures. The crack bridging effect diminishes the creation and spread of fractures, enabling the concrete cylinders to persistently withstand axial loads, even when cracks are present [35]. Despite the fact that PPF fibers are shorter, have a lower elasticity modulus, and have a lower tension strength in comparison to SF fibers, they possess the capability to bridge microcracks, as observed in previous studies (e.g., previous studies [19,36,37]).

3.5 Influence of strengthening on the initial stiffness

The distribution of loads in RC structures is greatly affected by the stiffness of the RC elements. Thus, it is essential that the technique used to strengthen RC elements that have been heat damaged return their compressive strength as well as their stiffness. To have a better understanding of how high temperatures and CFRP jacketing affect the elasticity of the concrete mixtures, it is important to assess the initial stiffness of the concrete cylinders. The initial stiffness was determined by dividing the stress by the axial strain at 40% of the maximum load. No cracks were seen in the concrete cylinders at this load level. Table 5 presents the experimental test results for the compressive strength and initial stiffness of all concrete cylinders. Table 5 and Figure 7 demonstrate that the heat-damaged concrete cylinders had a notable decrease in their initial stiffness. When subjected to 600°C, they caused a decrease in initial stiffness when CFRP jacketing was used and fibers were present. The heat-damaged concrete cylinders exhibited a decreased ratio in the initial stiffness up to 89.2% in comparison to the unheated concrete cylinders. Nevertheless, strengthening the heat-damaged cylinders resulted in an increase in the initial stiffness in comparison to the heat-damaged

Specimens	Compressive strength (MPa)	f_{cc}/f_c*	Relative difference (%) **	Initial stiffness (N/mm)	Relative difference (%)*
C0-A	30.2	—	—	20133.3	—
C0-T	14.1	—	−53.3	2169.2	−89.2
C0-A-S	48.1	1.59	+59.1	34945.5	+73.6
C0-T-S	30.2	2.14	+0.1	2419.3	−88.0
SF-A	40.7	—	—	26688.5	—
SF-T	28.5	—	−30.0	4560.0	−82.9
SF-A-S	56.7	1.39	+39.3	32400.0	+21.4
SF-T-S	43.6	1.53	+7.2	8729.1	−67.3
PPF-A	32.9	—	—	43866.7	—
PPF-T	18.0	—	−45.3	3600.0	−85.0
PPF-A-S	50.7	1.54	+54.1	33800.0	+41.3
PPF-T-S	35.3	1.96	+7.2	4029.4	−83.2
SF + PPF-A	40.5	—	—	27000.0	—
SF + PPF-T	30.9	—	−23.7	4414.3	−83.7
SF + PPF-A-S	53.5	1.32	+32.1	35666.7	+32.1
SF + PPF-T-S	40.1	1.30	−1.1	5342.0	−80.2

*f_{cc}/f_c is the confinement effectiveness ratio.
**The control specimen in each mixture is used as a reference specimen. A "+" sign refers to an increase, whereas a "−" sign refers to a reduction.
Table 5. Summary of experimental test results.

cylinders before strengthening. As an illustration, the stiffness of the cylinder was 8729.1 N/mm when SF was present, whereas it was 4560.0 N/mm before strengthening, with an increase of 91.4%. In addition, the inclusion of fibers improves the initial stiffness at ambient temperature by up to 34.1% in comparison to the C0-A cylinders (i.e., control concrete cylinders). Furthermore, a similar pattern was observed while employing CFRP jacketing to strengthen the concrete cylinders. The C0-A-S, SF-A-S, PPF-A-S, and SF + PPF-A-S exhibited a higher ratio of 73.6, 60.9, 67.9, and 77.2%, respectively, in comparison to the C0-A cylinders (i.e., control concrete cylinders). Cylinders' stiffness within the elastic zone depends on the CFRP's elastic modulus and confinement strength. The reduced initial stiffness of heat-damaged cylinders is mainly ascribed to the formation of micro-cracks due to the high temperature and the subsequent water evaporation, resulting in the softening and formation of pores in the concrete. As a result, when cylinders are compressed in the axial direction, heat-damaged cylinders are expected to exhibit a higher degree of lateral expansion compared to unheated concrete cylinders [38].

4. FE modeling

FE models were conducted using the commercial FE program ABAQUS [39] to conduct numerical analysis of concrete cylinders in exposure to heating scenarios and strengthen them with CFRP strips. The FE analytic approach comprises two consecutive steps: heat transfer and structural analysis. First, to examine the exposure to heating scenarios, a heat transfer analysis was carried out to evaluate the behavior of the concrete cylinders. Subsequently, the structural analysis, which is the second step, is carried out to examine the compressive behavior after the temperature influence produced in the heat transfer analysis (i.e., the first step). The ABAQUS/Explicit Solver was adopted to conduct this style of analysis.

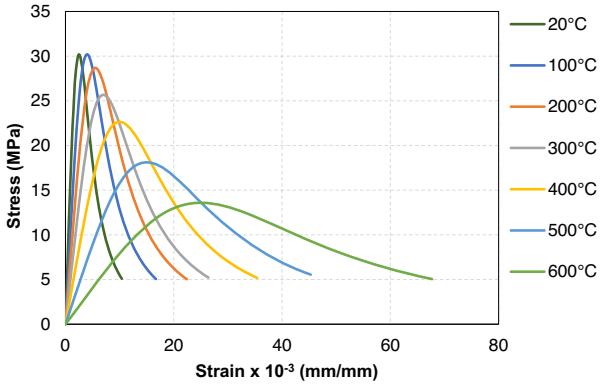

(a)

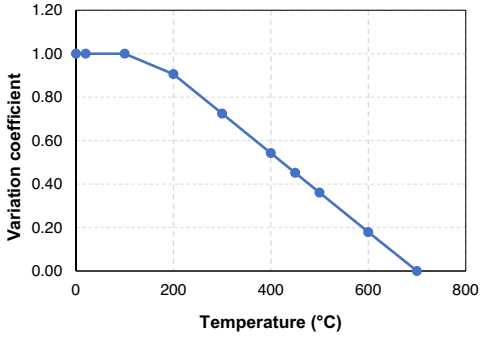

(b)

Figure 10. The concrete's mechanical properties at various temperatures: (a) stress–strain curves for unconfined deep beam (C0-A) and (b) reduction coefficient for modulus of elasticity.

4.1 Structural and temperature field analysis

In the first analysis step, thermal loading is performed based on the experimental heating curve (Figure 4) for heat transfer analysis. Each FE model is initially assigned an ambient temperature of 26°C. The heating curve was implemented using a tabular amplitude. Figure 4 demonstrates that the heating scenario is being studied for a duration of 3 h after reaching 600°C, representing the heating phase. Subsequently, the cooling phase commenced until reaching ambient temperatures. Employing a direct solution for conducting real-time fire analysis is time-consuming and resource-intensive. Because the loading and heating processes are quasi-static, the analysis can be accelerated by scaling in real-time. Rackauskaite et al. [40] have thoroughly examined the scaling factor. In this work, the analysis time is scaled by a factor of 100, a commonly utilized practice in previous studies [41,42]. Using the ABAQUS/Explicit Solver, a nonlinear FE structural analysis was carried out. Large displacement effects, materials, and geometrical elements are the nonlinear aspects of this technique. The experimental procedure is represented using push-down analysis with smooth displacement control. In order to avoid ABAQUS from assuming zero by default, the temperature is set in this step to 26°C, which is the ambient temperature. Furthermore, the total kinetic energy of the FE model remains below 5% of its internal energy. During a quasi-static loading procedure, the analysis job performed by external forces alters the FE system's kinetic and internal energies. In the initial loading stage, the FE system's kinetic energy may be comparatively high relative to its internal energy; however, as deformation progresses, a portion of the kinetic energy is transformed into internal energy [43]. As per the ABAQUS manual [39], to achieve the quasi-static condition of the entire loading procedure, the kinetic energy of the deforming FE model must remain below a negligible proportion of its total kinetic energy. The kinetic energy consistently remains below 5% of the internal energy during the entire response procedure, thereby validating the quasi-static FE simulation. The influence of elevated temperatures is generated in the study through sequentially coupled analysis, and in the subsequent steps of the structural analysis, it is specified as a predefined field.

	Parameters		Value
Elastic properties	Poisson's ratio	N	0.3
	Elastic modulus	E_1 (MPa)	220
		E_2 (MPa)	10
	Modulus of rigidity	G_{12} =	5
		G_{13} (MPa)	
CFRP strength	Tensile strength	f_{t1} (MPa)	3,000
		f_{t2} (MPa)	12
	Compressive strength	f_{c1} =	12
		f_{c2} (MPa)	
	Shear strength	V_{f1} =	12
		V_{f2} (MPa)	
Damage evolution	Tensile fracture energy	G_{t1} (mJ/mm^2)	95
		G_{t2} (mJ/mm^2)	1.2
	Compressive fracture energy	G_{c1} (mJ/mm^2)	95
		G_{c2} (mJ/mm^2)	1.2

Table 7. Parameter values of CFRP material characteristics in this study.

4.2 Constitutive material models

4.2.1 Temperature-dependent material characteristics

The thermal properties of concrete material include the thermal expansion coefficient, specific heat capacity, and thermal conductivity. The present investigation utilized the temperature-dependent specific heat capacity and thermal expansion coefficient suggested by Eurocode 2 [44] for concrete, as depicted in Figure 9(a) and (b). In addition, the upper limit for the thermal conductivity values for concrete, as specified in Eurocode 2 [44], was utilized, as depicted in Figure 9(c).

Parameters	Dilation angle (°)	Potential eccentricity	Biaxial to uniaxial compressive strengths	Compressive meridian	Viscosity parameter
Unconfined concrete	30	0.1	1.16	0.7	0
Confined concrete	15	0.1	1.16	0.7	0

Table 6. Parameter values of concrete damaged plasticity model in this study.

4.2.2 Mechanical properties

The concrete materials' properties incorporate the modulus of elasticity and the stress–strain relationship. The stress–strain relationship of unconfined concrete, as specified by Eurocode 2 [44], was adopted. For example, Figure 10(a) illustrates these relationships for unconfined deep beams (C0-A). Furthermore, the coefficient of temperature-dependent variation specified in Eurocode 2 [44] for the elastic modulus of the concrete was adopted, as depicted in Figure 10(b). Temperature independence was assumed for the mass density and Poisson's ratio of the concrete. The concrete density was established at 2,400 kg/m^3, while Poisson's ratio was assumed to be 0.2 for all temperatures. Regarding modeling strengthened deep beams, it is recommended to represent the concrete material as a confined material. Therefore, it is essential to transform the experimental stress–strain curves for the unconfined concrete curves (at 26°C) into confined curves. This study used the concrete material's confined stress–strain curve as described in previous studies [45,46]. The concrete damaged plasticity model was utilized in this study to simulate the plasticity behavior of both confined and unconfined concretes. Table 2 displays the parameter values necessary for the concrete damaged plasticity model [39]. The tensile behavior typically has less significance in simulating confined concrete [1], while it has significance in the presence of fibers. Nevertheless, it was assumed that the tension's stress–strain curve exhibited linear elasticity until reaching the tensile strength, which is 10% of the compressive strength. Subsequently, there was a significant linear decline in stress until it reached zero. To mitigate FE analysis instability, the constitutive model incorporated 1% of the tensile strength rather than zero (Table 6).

The CFRP strips were characterized in ABAQUS as a "Lamina" material type having a linear elastic response that can be simulated using the ABAQUS software. The experimental findings indicated that the CFRP strips failed due to tension rupture. Therefore, it is necessary to accurately represent the damage characteristics of the CFRP strips in the nonlinear FE model. To accurately characterize the behavior of CFRP, it is essential to specify the elastic behavior of the laminate, its ultimate strength, and

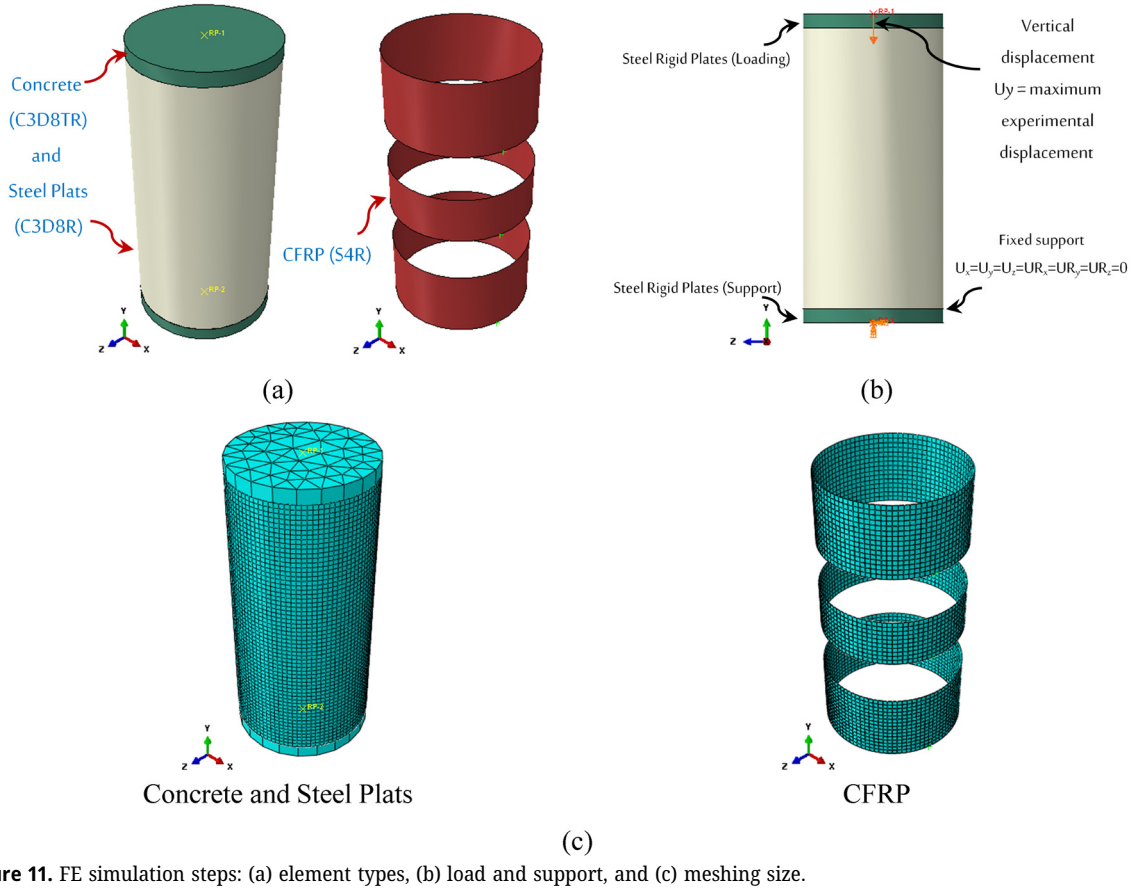

Figure 11. FE simulation steps: (a) element types, (b) load and support, and (c) meshing size.

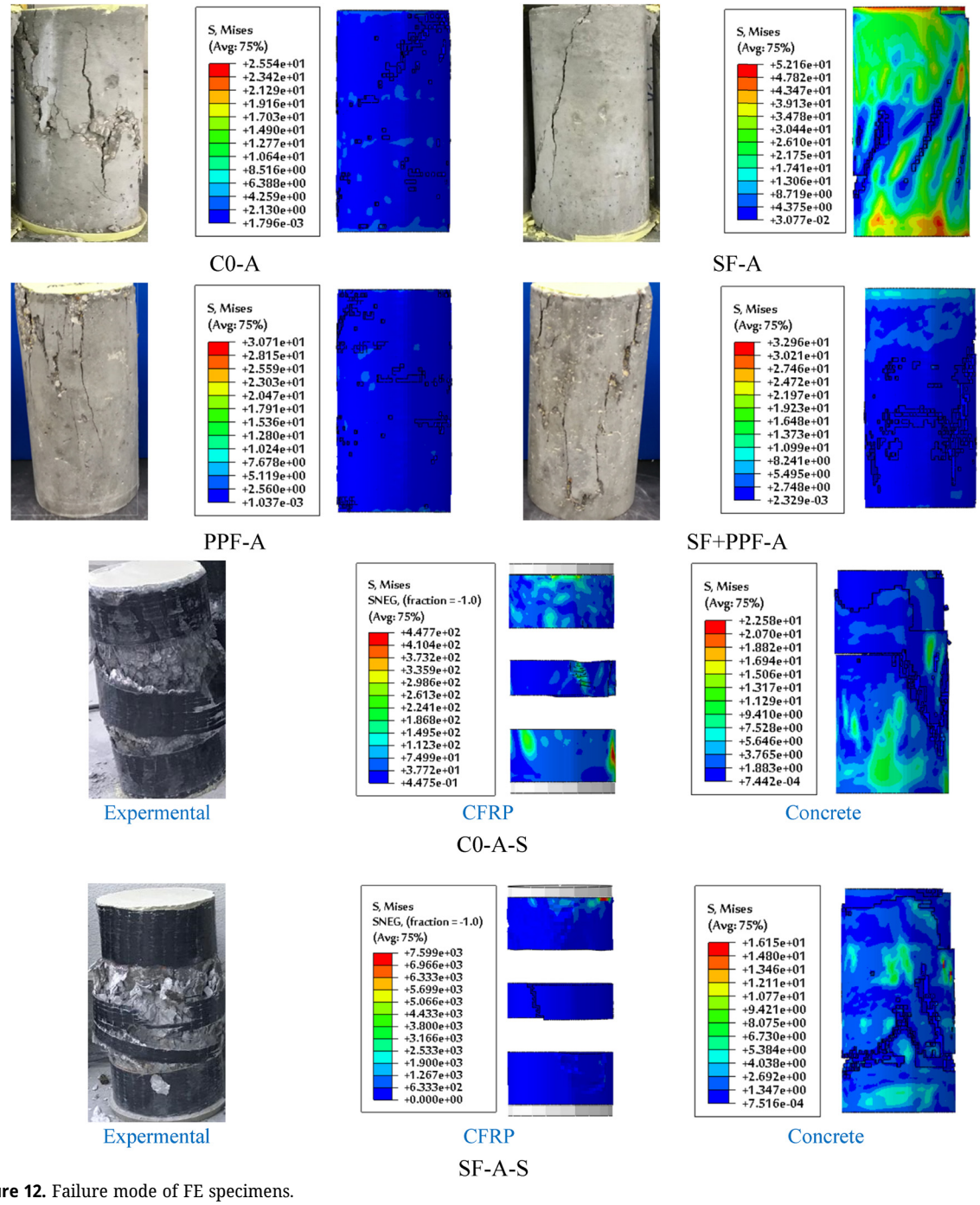

Figure 12. Failure mode of FE specimens.

the attributes related to the evolution of damage. The perpendicular characteristics of CFRP were considered to have low values, as reported in previous studies [47–49]. The Hashin Damage Model, implemented in ABAQUS, was utilized to simulate the ultimate strength and damage characteristics [50]. Table 7 presents the attributes of the CFRP strips. In Table 7, subscripts 1 and 2 represent the orientation of the carbon fibers and the vertical direction, respectively. The fracture energies were obtained from the study of Shi et al. [51].

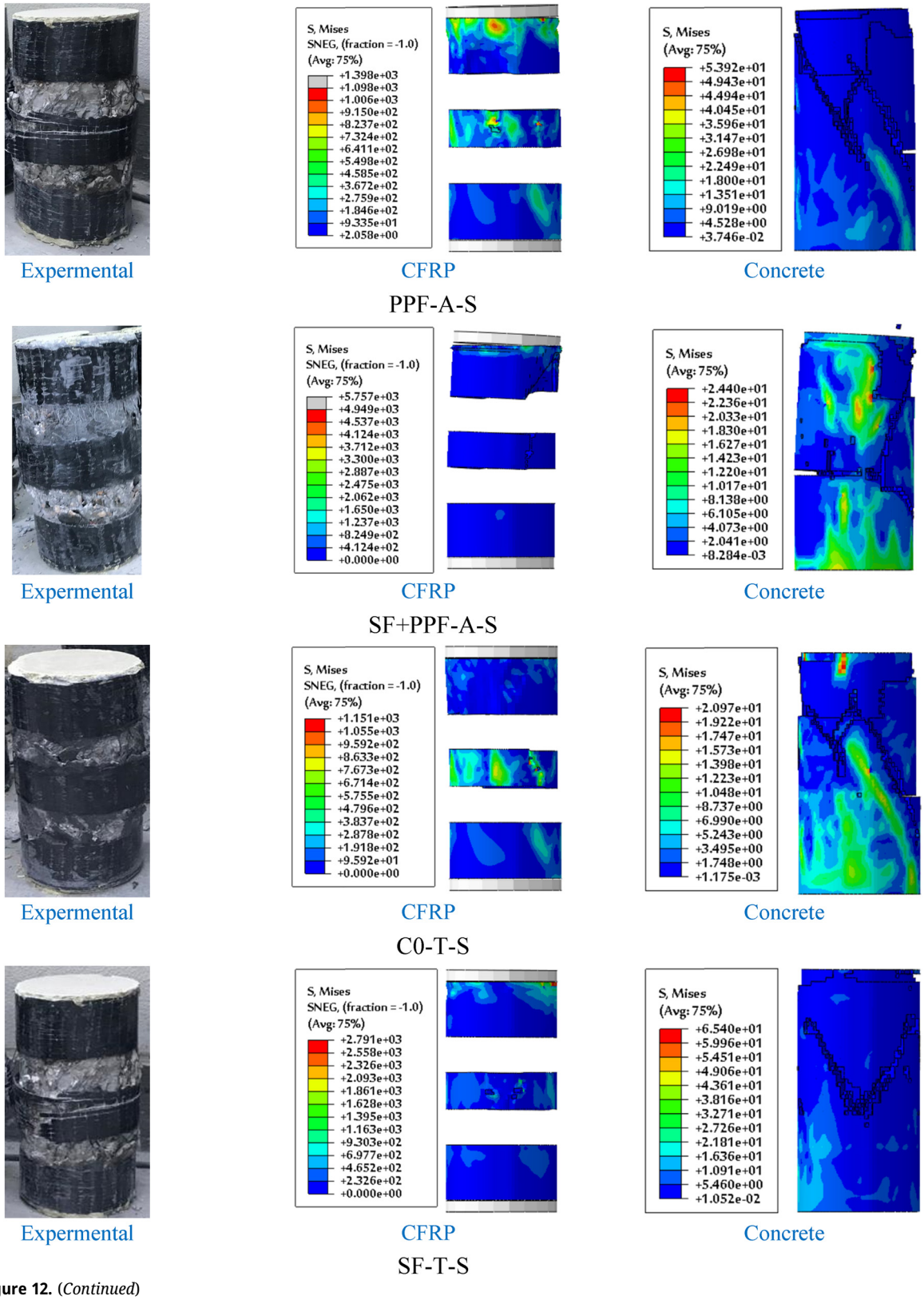

Figure 12. (*Continued*)

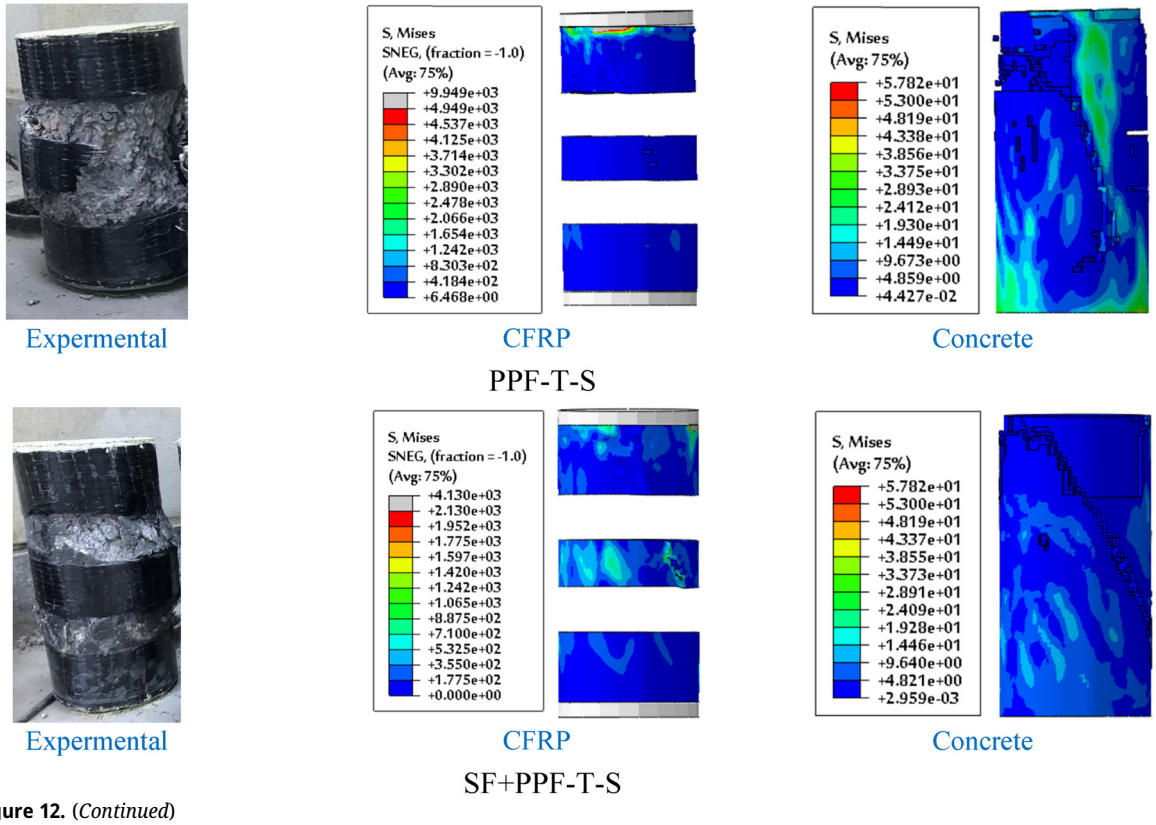

Figure 12. (*Continued*)

4.3 FE modeling

The thermal and structural FE analysis elements for concrete are conducted utilizing the C3D8TR 8-node elements, which are thermally connected and have trilinear displacement, temperature, and decreased integration properties, as shown in Figure 11(a). For the steel plates, a C3D8R element was used. The CFRP strips were simulated using a 4-node shell element with a reduced integration element (S4R). The reference points (RPs) that are linked to the lower supporting plate are shown in Figure 11(b). This position was utilized to apply a boundary condition (i.e., fixed support). The RP assigned to the top plate was utilized for the load application (i.e., displacement control), as depicted in Figure 11(b). The interaction between the concrete cylinder and the CFRP strip was modeled as a surface tie constraint, where the concrete cylinder's surface served as the master surface, and the slave surface was chosen for the inner surface of the CFRP shell, which was widely used in FE analysis [52]. A general contact model was used to model the contact between the steel plates and the concrete cylinder. This work uses hard contact to model the interaction properties, specifically the interaction in the normal and tangential directions. The friction coefficient of 0.47 is applied to the concrete cylinder's surface and the steel plates. Finally, a mesh that is uniform with a size of 5 mm was selected due to its satisfactory performance compared to the experimental results, as depicted in Figure 11(c).

4.4 Validation of the FE model result

This section provides an FE verification of the experimental findings. Figure 12 and Table 8 show the failure patterns and the compressive strength of the FE models in comparison with the experimental outcomes, respectively. The FE models have successfully predicted the failure patterns observed in experimental tests of FRC cylinders while strengthening by CFRP strips after exposure to heating. The deformation patterns and stress graphs (referred to as "S, Mises" for concrete and "S, Mises-SNEG" for CFRP strips) observed in the FE models are consistent with the experimental outcomes. There is a satisfactory agreement between the FE analysis and the experimental outcomes. Table 8 demonstrates that the FE model effectively captures the

Specimens ID	Compressive strength (MPa)		Experimental/FE
	Experimental	FE	
C0-A	30.2	31.3	1.04
C0-T	14.1	15.2	1.08
C0-A-S	48.1	51.7	1.07
C0-T-S	30.2	32.1	1.06
SF-A	40.7	43.1	1.06
SF-T	28.5	30.5	1.07
SF-A-S	56.7	59.4	1.05
SF-T-S	43.6	46.9	1.08
PPF-A	32.9	34.7	1.05
PPF-T	18.0	19.8	1.10
PPF-A-S	50.7	54.3	1.07
PPF-T-S	35.3	38.4	1.09
SF + PPF-A	40.5	43.8	1.08
SF + PPF-T	30.9	34.1	1.10
SF + PPF-A-S	53.5	58.4	1.09
SF + PPF-T-S	40.1	44.2	1.10

Table 8. FE and experimental test results.

compressive strength observed in the experimental test. The disparity between the actual experimental results and the simulated FE model is within a satisfactory range. Table 8 illustrates that the highest disparity was around 10%. There were certain differences between the experimental specimens and the simulated FE models. The observed disparity between the failure patterns and compressive strength can be explained by the FE specimens' flawless performance throughout the analysis. The initial concrete flaws, such as lack of uniformity and premature cracking, could not be completely represented by the simulated FE model. In summary, the simulations presented sufficient proof that the FE models are dependable, thereby confirming their suitability for generating additional predictions.

5. Conclusion

In this study, the compressive strength of FRC specimens strengthened with CFRP strips after exposure to heating was experimentally and numerically investigated. The main conclusions of the present investigation can be summarized as follows:

1. After exposure to a temperature of 600°C, the compressive strengths decreased by a range of 23.7–53.3% for both plain and FRC specimens.
2. The presence of fibers significantly impacted compressive strength, regardless of the fiber type, leading to an enhanced ratio of up to 34.7%.
3. The strengthened cylinders showed higher compressive strength compared to the unstrengthened cylinders. The unheated strengthened cylinders showed an increased ratio of 32.1–59.1%, while the heated strengthened cylinders showed an increased ratio of 29.8–114.2%.
4. The heat-damaged concrete cylinders had higher failure rates than the unheated cylinders. Fibers in mixtures reduced surface thermal cracks and improved toughness, altering the failure pattern from brittle to ductile. Strengthening heat-damaged cylinders did not significantly influence the eventual failure mode.
5. The utilization of CFRP jackets significantly improved the peak strength, strain at peak stress, and post-peak behavior of all specimens, irrespective of whether the concrete cylinders were heated or unheated.
6. Fibers significantly influence compressive strength, reducing the negative impact of exposure to 600°C. SF and hybrid reinforced fiber concrete cylinders show superior performance compared to other mixtures under strengthened and unstrengthened conditions.
7. Heat-damaged cylinders had reduced initial stiffness ratios by up to 89.2% compared to unheated cylinders. The strengthening of the heat-damaged cylinders resulted in an increase in the initial stiffness up to 91.4% in comparison to the heat-damaged cylinders before strengthening.
8. The simulated FE model used in this study successfully simulated the compressive strength and failure pattern of FRC cylinders strengthened with CFRP strips. The results of the simulated FE model showed satisfactory agreement with experimental data, indicating that the simulated FE model is effective in representing the plastic behavior of CFRP-confined concrete.
9. The use of CFRP strips to upgrade heat-damaged concrete cylinders has shown promise in terms of regaining structural integrity and preventing the Poisson effect of concrete. This approach is a good option for fixing damaged concrete structures since it is simple and

economical to apply and CFRP strips operate well in harsh environments and are more economical than fully CFRP wrapping.

The authors recommend the use of SF, which demonstrated remarkable stability and durability when subjected to high temperatures. Furthermore, it demonstrated excellent efficiency when strengthened by CFRP strips.

Acknowledgements

The authors extend their appreciation to the Researchers Supporting Project (number RSP2024R343), King Saud University, Riyadh, Saudi Arabia.

Author contributions

Aref A. Abadel: Conceptualization, Methodology, Formal analysis, Investigation, Data curation, Visualization, Fund acquisition, Project administration, Writing Original draft, Writing Review and Editing. Yousef R. Alharbi: Formal analysis, Investigation, Data curation, Visualization, Writing Original draft, Writing Review and Editing.

Conflict of interest statement

The authors state no conflict of interest.

References

[1] Totonchi, A., Ansaripour, A., Shivaei, S., Effect of different arrangements of CFRP wraps on the axial stress–strain behaviour of confined concrete cylinders: Experimental study and numerical modelling, Iran. J. Sci. Technol. Trans. Civ. Eng., 2020, 44(4): 1087–1100

[2] Sarker, P.K., Kelly, S., Yao, Z., Effect of fire exposure on cracking, spalling and residual strength of fly ash geopolymer concrete, Mater. Des., 2014, 63: 584–592

[3] Shaikh, F.U.A., Vimonsatit, V., Effect of cooling methods on residual compressive strength and cracking behavior of fly ash concretes exposed at elevated temperatures, Fire Mater., 2016, 40(2): 335–350

[4] Abadel, A., Elsanadedy, H., Almusallam, T., Alaskar, A., Abbas, H., Al-Salloum, Y., Residual compressive strength of plain and fiber reinforced concrete after exposure to different heating and cooling regimes, Eur. J. Environ. Civ. Eng., 2022, 26(14): 6746–6765

[5] Li, Q., Yuan, G., Shu, Q., Effects of heating/cooling on recovery of strength and carbonation resistance of fire-damaged concrete, Mag. Concr. Res., 2014, 66(18): 925–936

[6] Kee, S.-H., Kang, J.W., Choi, B.-J., Kwon, J., Candelaria, M.D., Evaluation of static and dynamic residual mechanical properties of heat-damaged concrete for nuclear reactor auxiliary buildings in korea using elastic wave velocity measurements, Materials, 2019, 12(17): 2695

[7] Choe, G., Kim, G., Gucunski, N., Lee, S., Evaluation of the mechanical properties of 200 MPa ultra-high-strength concrete at elevated temperatures and residual strength of column, Constr. Build. Mater., 2015, 86: 159–168

[8] Gong, W., Ueda, T., Basic study on chloride-induced steel corrosion in concrete subjected to heating up to 300° C, Material., 2018, 67(7): 738–745

[9] Khaliq, W., Kodur, V., Thermal and mechanical properties of fiber reinforced high performance self-consolidating concrete at elevated temperatures, Cem. Concr. Res., 2011, 41(11): 1112–1122

[10] Novák, J., Kohoutková, A.J.P.E., Fire response of hybrid fiber reinforced concrete to high temperature, Procedia Eng., 2017, 172: 784–790

[11] Peng, G.-F., Bian, S.-H., Guo, Z.-Q., Zhao, J., Peng, X.-L., Jiang, Y.-C., Effect of thermal shock due to rapid cooling on residual mechanical properties of fiber concrete exposed to high temperatures, Constr. Build. Mater., 2008, 22(5): 948–955

[12] Vairagade, V.S., Dhale, S.A., Hybrid fibre reinforced concrete–a state of the art review, Hybrid. Adv., 2023, 3: 100035

[13] Abadel, A., Abbas, H., Almusallam, T., Al-Salloum, Y., Siddiqui, N., Mechanical properties of hybrid fibre-reinforced concrete–analytical modelling and experimental behaviour, Mag. Concr. Res., 2016, 68(16): 823–843

[14] Selvi, M.T., Thandavamoorthy, T.S., Load-deflection characteristics of steel, polypropylene and hybrid fiber reinforced concrete beams, Arch. Civ. Eng., 2015, 61(1): 59–72

[15] Marcalikova, Z., Mateckova, P., Racek, M., Bujdos, D., Study on shear behavior of steel fiber reinforced concrete small beams, Procedia Struct. Integr., 2020, 28: 957–963

[16] Brandt, A.M. Cement-based composites: materials, mechanical properties and performance, CRC Press, London, 2005

[17] Sharma, A., Reddy, G.R., Varshney, L., Bharathkumar, H., Vaze, K.K., Ghosh, A.K., et al., Experimental investigations on mechanical and radiation shielding properties of hybrid lead–steel fiber reinforced concrete, Nucl. Eng. Des., 2009, 239(7): 1180–1185

[18] Shu, X., Graham, R.K., Huang, B., Burdette, E.G., Hybrid effects of carbon fibers on mechanical properties of Portland cement mortar, Mater. Des. (1980-2015), 2015, 65: 1222–1228

[19] Alwesabi, E.A.H., Bakar, B.H.A., Alshaikh, I.M.H., Akil, H.M., Experimental investigation on mechanical properties of plain and rubberised concretes with steel–polypropylene hybrid fibre, Constr. Build. Mater., 2020, 233: 117194

[20] Alwesabi, E.A.H., Bakar, B.H.A., Alshaikh, I.M.H., Zeyad, A.M., Altheeb, A., Alghamdi, H., Experimental investigation on fracture characteristics of plain and rubberized concrete containing hybrid steel-polypropylene fiber, Structures, 33: 4421–4432

[21] Abadel, A., Abbas, H., Almusallam, T., Alshaikh, I.M.H., Khawaji, M., Alghamdi, H., et al., Experimental study of shear behavior of CFRP strengthened ultra-high-performance fiber-reinforced concrete deep beams, Case Stud. Constr. Mater., 2022, 16: e01103

[22] Abadel, A.A., Retrofitting of heat-damaged fiber-reinforced concrete cylinders using welded wire mesh configurations, Mater. Sci. Poland, 2024, 42(2): 52–69

[23] Ali Ahmed, C., Si Salem, A., Ait Taleb, S., Ait Tahar, K., Experimental behavior and reliability of predamaged concrete columns externally repaired with FRP spiral strips under axial compression, World J. Eng., 2024, 21(1): 115–126

[24] Varma, D.A., Joseph, L., Madhavan, M.K., Jayanarayanan, K., Pegoretti, A., Strength, durability and finite element analysis of hybrid jute/basalt fiber reinforced polymer confined concrete column under axial compression, Results Eng., 2024, 22: 102281

[25] Dushimimana, A., Vassilopoulos, A.P., Sena-Cruz, J., Pereira, J.M., Correia, L., Cabral-Fonseca, S., et al., Behavior of CFRP composites and epoxy adhesives after long-term exposure to outdoor and laboratory-controlled environments, Constr. Build. Mater., 2024, 438: 137201

[26] Das Chandra, S., Nizam, Md.E.H., Applications of fiber reinforced polymer composites (FRP) in civil engineering, Int. J. Adv. Struct. Geotech. Eng., 2014, 3(3): 299–309

[27] Rahman, A., Mallick, M., Ghosh, S., Experimental behavior of FRP confined concrete cylinder wrapped by two different FRPs, J. Mater. Sci. Res., 2018, 7(2): 18–25

[28] Wang, Z., Wang, D., Smith, S.T., Lu, D., CFRP-confined square RC columns. I: experimental investigation, J. Compos. Constr., 2012, 16(2): 150–160

[29] Xiang, Z., Tong, Y., Niu, J., Yin, L., Zhou, J., Experimental study on the axial compressive mechanical performance of concrete short columns jointly confined with CC and CFRP after sulfate attack, J. Build. Eng., 2024, 95: 110342

[30] ASTM, D3039/D3039M-08, Standard test method for tensile properties of polymer matrix composite materials, American Society for Testing and Materials, West Conshohocken, PA, 2008

[31] ISO, 834: fire resistance tests-elements of building construction, Geneva, Switzerland, International Organization for Standardization, 1999

[32] ASTM, C39, Standard test method for compressive strength of cylindrical concrete specimens, standard, West Conshohocken, ASTM International, 2012

[33] Al-Salloum, Y.A., Almusallam, T.H., Elsanadedy, H.M., Iqbal, R.A., Effect of elevated temperature environments on the residual axial capacity of RC columns strengthened with different techniques, Constr. Build. Mater., 2016, 115: 345–361

[34] Elsanadedy, H., Almusallam, T., Al-Salloum, Y., Iqbal, R., Effect of high temperature on structural response of reinforced concrete circular columns strengthened with fiber reinforced polymer composites, J. Compos. Mater., 2017, 51(3): 333–355

[35] Alshaikh, I.M.H., Abu Bakar, B.H., Alwesabi, E.A.H., Abadel, A.A., Alghamdi, H., Wasim, M., An experimental study on enhancing progressive collapse resistance using a steel fiber–reinforced concrete frame, J. Struct. Eng., 2022, 148(7): 04022087

[36] Alwesabi, E.A., Bakar, B.H.A., Alshaikh, I.M.H., Akil, H.M., Impact resistance of plain and rubberized concrete containing steel and polypropylene hybrid fiber, Mater. Today Commun., 2020, 25: 101640

[37] Alwesabi, E.A.H., Bakar, B.H.A., Alshaikh, I.M.H., Abadel, A.A., Alghamdi, H., Wasim, M., An experimental study of compressive toughness of steel–polypropylene hybrid fibre-reinforced concrete, Structures, 37: 379–388

[38] Abadel, A.A., Masmoudi, R., Khan, M.I., Axial behavior of square and circular concrete columns confined with CFRP sheets under elevated temperatures: comparison with welded-wire mesh steel confinement, Structures, 45: 126–144

[39] ABAQUS, User assistance, Rhode Island, USA, Dassault Systemes Simulia Corporation, Providence, 2019
[40] Rackauskaite, E., Kotsovinos, P., Rein, G.J.F.S.J., Model parameter sensitivity and benchmarking of the explicit dynamic solver of LS-DYNA for structural analysis in case of fire, Fire Saf. J., 2017, 90: 123–138
[41] Alshaikh, I.M.H., Abadel, A.A., Tuladhar, R., Alwathaf, A.H., Nehdi, M.L., Progressive collapse resistance of post-fire cellular beam-column substructures with various web-opening shapes, Structures, 55: 1874–1893
[42] Ma, Z., Havula, J., Heinisuo, M., Structural fire analysis of simple steel structures by using LS-DYNA explicit solver, Rakenteiden Mekaniikka, 2019, 52(1): 1–22
[43] Li, Z., Zhu, Y.F., Zhang, H., Liu, Y., Yao, Y., Progressive collapse resistance of self-resilient composite frames under fire conditions, Structures, 2024, 68: 107127
[44] Eurocode-2, Design of concrete structures-part 1-2: General rules-structural fire design, European Committee for Standardization, Brussels, 2004
[45] Hu, H.-T., Huang, C.-S., Wu, M.-H., Wu, Y.-M., Nonlinear analysis of axially loaded concrete-filled tube columns with confinement effect, J. Struct. Eng., 2003, 129(10): 1322–1329
[46] Sadeghian, P., Rahai, A.R., Ehsani, M.R., Numerical modeling of concrete cylinders confined with CFRP composites, J. Reinf. Plast. Compos., 2008, 27(12): 1309–1321
[47] Al-Mekhlafi, G.M., Al-Osta, M.A., Sharif, A.M., Behavior of eccentrically loaded concrete-filled stainless steel tubular stub columns confined by CFRP composites, Eng. Struct., 2020, 205: 110113
[48] Hany, N.F., Hantouche, E.G., Harajli, M.H., Finite element modeling of FRP-confined concrete using modified concrete damaged plasticity, Eng. Struct., 2016, 125: 1–14
[49] Sharif, A.M., Al-Mekhlafi, G.M., Al-Osta, M.A., Structural performance of CFRP-strengthened concrete-filled stainless steel tubular short columns, Eng. Struct., 2019, 183: 94–109
[50] Hashin, Z., Failure criteria for unidirectional fiber composites, J. Appl. Mech., 1980, 47(2): 329–334
[51] Shi, Y., Swait, T., Soutis, C., Modelling damage evolution in composite laminates subjected to low velocity impact, Compos. Struct., 2012, 94(9): 2902–2913
[52] Alshaikh, I.M.H., Nehdi, M.L., Abadel, A.A., Numerical investigations on progressive collapse of rubberized concrete frames strengthened by CFRP sheets, Structures, 2024, 60: 105918